Contents

1

DRMG applied to two-dimensional classical lattice models

1.1 Abstract

This chapter explains how to apply to ideas of the density matrix renormalization group to two-dimensional classical lattices. The Ising model is used throughout.

First, we explain the transfer-matrix formulation for classical partition functions.

Then, we show how to renormalize the transfer matrix using DMRG. This was first done by Nishino [1]. To make notation easier, we redefine the transfer matrix in terms of a tensor network.

Then, we explain the corner transfer matrix renormalization group. This method, first introduced by Nishino and Okunishi [2], combines ideas from Baxter [**baxter1982exactly**, 3, 4] and White [5] to significantly speed up the renormalization of the transfer matrix.

1.2 Partition functions of classical lattices

The central quantity in equilibrium statistical mechanics is the partition function Z, which, for a discrete system such as a lattice, is defined as

$$Z = \sum_s \exp\left(-\beta H(s)\right), \tag{1.1}$$

where the sum is over all microstates s, H is the energy function, and $\beta = T^{-1}$ the inverse temperature.

1.3 Transfer matrices of lattice models

Transfer matrices are used to re-express the partition function of classical lattice systems, allowing them to be solved exactly or approximated.

We will introduce the transfer matrix in the context of the 1D classical Ising model, first introduced and solved using the transfer matrix method by Ising [6] in his PhD thesis.

1.3.1 1D Ising model

talk a bit about model (magnetism etc).

Somewhere, I should introduce – very briefly – how the magnetization and free energy per site are defined. Maybe just calculate them for 1D Ising model.

Consider the 1D zero-field ferromagnetic Ising model [6], defined by the energy function

$$H(\sigma) = -J \sum_{\langle ij \rangle} \sigma_i \sigma_j. \tag{1.2}$$

Here, we sum over nearest neighbors $\langle ij \rangle$ and the spins σ_i take the values ± 1. $J > 0$.

Assume, for the moment, that the chain consists of N spins, and apply periodic boundary conditions. The partition function of this system is given by

$$Z_N = \sum_{\sigma_1, \ldots, \sigma_N \in \{-1,1\}} \exp(-\beta H(\sigma)) \tag{1.3}$$

Exploiting the local nature of the interaction between spins, we can write

$$Z_N = \sum_{\sigma_1, \cdots, \sigma_N \in \{-1,1\}} \prod_{\langle i,j \rangle} e^{K \sigma_i \sigma_j} \tag{1.4}$$

where we defined $K \equiv \beta J$.

Now, we define the 2×2 matrix

$$T_{\sigma\sigma'} = \exp(K\sigma\sigma'). \tag{1.5}$$

A possible choice of basis is

$$(|\uparrow\rangle = 1, |\downarrow\rangle = -1) = \left(\begin{bmatrix} 1 \\ 0 \end{bmatrix}, \begin{bmatrix} 0 \\ 1 \end{bmatrix}\right). \tag{1.6}$$

In terms of this matrix, Z_N is written as

$$Z_N = \sum_{\sigma_1,\cdots,\sigma_N} T_{\sigma_1\sigma_2}\cdots T_{\sigma_N\sigma_1} = \mathrm{Tr}\, T^N. \tag{1.7}$$

T is called the transfer matrix. In the basis of Equation 1.6, T is written as

$$T = \begin{bmatrix} e^K & e^{-K} \\ e^{-K} & e^{-K} \end{bmatrix}. \tag{1.8}$$

T is, in fact, diagonalizable. So, we can write $T^N = PD^NP^{-1}$, where P consists of the eigenvectors of T, and D has the corresponding eigenvalues on the diagonal. By the cyclic property of the trace, we have

$$Z_N = \lambda_1^N + \lambda_2^N, \tag{1.9}$$

where

$$\lambda_1 = e^K + e^{-K},$$
$$\lambda_2 = e^K - e^{-K}.$$

Thus, we have reduced the problem of finding the partition function to an eigenvalue problem.

In the thermodynamic limit $N \to \infty$

$$Z = \lim_{N\to\infty} \lambda_1^N \tag{1.10}$$

where λ_1 is the non-degenerate largest eigenvalue (in absolute value) of T.

Fixed boundary conditions

We may also apply fixed boundary conditions. The partition function is then written as

$$Z_N = \langle \sigma' | \, T^N \, | \sigma \rangle, \tag{1.11}$$

where $|\sigma\rangle$ and $|\sigma'\rangle$ are the right and left boundary spins.

In the large-N limit, T^N tends towards the projector onto the eigenspace spanned by the eigenvector belonging to the largest eigenvalue

$$|\lambda_1\rangle = \lim_{N\to\infty} \frac{T^N \, |\sigma\rangle}{\left\| T^N \, |\sigma\rangle \right\|}. \tag{1.12}$$

Equation 1.12 is true for any $|\sigma\rangle$ that is not orthogonal to $|\lambda_1\rangle$.

The physical significance of the normalized lowest-lying eigenvector $|\lambda_1\rangle$ is that $\langle\lambda_1|\uparrow\rangle$ and $\langle\lambda_1|\downarrow\rangle$ represent the Boltzmann weight of $|\uparrow\rangle$ and $|\downarrow\rangle$ at the boundary of a half-infinite chain.

Maybe picture of above claim?

1.3.2 2D Ising model

Talk about exact solution (Onsager). Why is it important? Maybe star-triangle relation (Baxter). Not all IRF models solvable.

Next, we treat the two-dimensional, square-lattice Ising model. In two dimensions, the energy function is still written as in Equation 1.2, but now every lattice site has four neighbors.

Let N be the number of columns and l be the number of rows of the lattice, and assume $l \gg N$. In the vertical direction, we apply periodic boundary conditions, as in the one-dimensional case. In the horizontal direction, we keep an open boundary. We refer to N as the system size.

Picture.

Similarly as in the 1D case, the partition function can be written as

$$Z_N = \sum_{\boldsymbol{\sigma}} \prod_{\langle i,j,k,l\rangle} W(\sigma_i, \sigma_j, \sigma_k, \sigma_l) \tag{1.13}$$

where the product runs over all groups of four spins sharing the same face. The Boltzmann weight of such a face is given by

$$W(\sigma_i, \sigma_j, \sigma_k, \sigma_l) = \exp\left\{\frac{K}{2}(\sigma_i\sigma_j + \sigma_j\sigma_k + \sigma_k\sigma_l + \sigma_l\sigma_i)\right\} \tag{1.14}$$

We can express the Boltzmann weight of a configuration of the whole lattice as a product of the Boltzmann weights of the rows

$$Z_N = \sum_{\boldsymbol{\sigma}} \prod_{r=1}^{l} W(\sigma_1^r, \sigma_2^r, \sigma_1^{r+1}, \sigma_2^{r+1}) \ldots W(\sigma_{N-1}^r, \sigma_N^r, \sigma_{N-1}^{r+1}, \sigma_N^{r+1}) \tag{1.15}$$

where σ_i^r denotes the value of the ith spin of row r.

Now, we can generalize the definition of the transfer matrix to two dimensions, by defining it as the Boltzmann weight of an entire row

$$T_N(\boldsymbol{\sigma}, \boldsymbol{\sigma'}) = W(\sigma_1, \sigma_2, \sigma'_1, \sigma'_2) \ldots W(\sigma_{N-1}, \sigma_N, \sigma'_{N-1}, \sigma'_N) \tag{1.16}$$

If we take the spin configurations of an entire row as basis vectors, T_N can be written as a matrix of dimensions $2^N \times 2^N$.

Similarly as in the one-dimensional case, the partition function now becomes

$$Z_N = \sum_{\boldsymbol{\sigma}} \prod_{r=1}^{l} T_N(\boldsymbol{\sigma}^r, \boldsymbol{\sigma}^{r+1}) = \mathrm{Tr}\, T_N^l \tag{1.17}$$

In the limit of an $N \times \infty$ cylinder, the partition function is once again determined by the largest eigenvalue[1].

$$Z_N = \lim_{l\to\infty} T_N^l = \lim_{l\to\infty} (\lambda_0)_N^l \tag{1.18}$$

The partition function in the thermodynamic limit is given by

$$Z = \lim_{N\to\infty} Z_N \tag{1.19}$$

1.4 Partition function of the 2D Ising model as a tensor network

In calculating the partition function of 1D and 2D lattices, matrices of Boltzmann weights like W and T play a crucial role. We have formulated them in a way that is valid for any interaction-round-a-face (IRF) model, defined by

$$H \sim \sum_{\langle i,j,k,l \rangle} W(\sigma_i, \sigma_j, \sigma_k, \sigma_l), \tag{1.20}$$

where the summation is over all spins sharing a face. W can contain 4-spin, 3-spin, 2-spin and 1-spin interaction terms. The Ising model is a special case of the IRF model, with W given by Equation 1.14.

We will now express the partition function of the 2D Ising model as a tensor network. The transfer matrix T is redefined in the process. This allows us to visualize the equations in a way that is consistent with the many other tensor network algorithms under research today. For an introduction to tensor network notation, see ??.

[1] As in the 1D case, T is symmetric, so it is orthogonally diagonalizable.

1.4.1 Tensor network of the partition function of a system of four spins

We define

$$Q(\sigma_i, \sigma_j) = \exp(K\sigma_i\sigma_j) \tag{1.21}$$

as the Boltzmann weight of the bond between σ_i and σ_j. It is the same as the 1D transfer matrix in Equation 1.5.

The Boltzmann weight of a face W decomposes into a product of Boltzmann weights of bonds

$$W(\sigma_i, \sigma_j, \sigma_k, \sigma_l) = Q(\sigma_i, \sigma_j)Q(\sigma_j, \sigma_l)Q(\sigma_l, \sigma_k)Q(\sigma_k, \sigma_i). \tag{1.22}$$

It is now easy to see that the partition function is equal to the contracted tensor network in Figure 1.1:

$$\begin{aligned} Z_{2\times 2} &= \sum_{\sigma_1,\sigma_2,\sigma_3,\sigma_4} \sum_{a,b,c,d} \delta_{\sigma_1,a}Q(a, b)\delta_{\sigma_2,b}Q(b, c)\delta_{\sigma_3,c}Q(c, d)\delta_{\sigma_4,d}Q(d, a) \\ &= \sum_{\sigma_1,\sigma_2,\sigma_3,\sigma_4} W(\sigma_1, \sigma_2, \sigma_3, \sigma_4). \end{aligned} \tag{1.23}$$

where the Kronecker delta is defined as usual:

$$\delta_{ij} = \begin{cases} 1 & \text{if } i = j \\ 0 & \text{if } i \neq j. \end{cases} \tag{1.24}$$

1.4.2 Thermodynamic limit

We define the matrix P by

$$P^2 = Q. \tag{1.25}$$

as in Figure 1.2. This allows us to write the partition function of an arbitrary $N \times l$ square lattice as a tensor network of a single recurrent tensor a_{ijkl}, given by

$$a_{ijkl} = \sum_{a,b,c,d} \delta_{abcd}P_{ia}P_{jb}P_{kc}P_{ld}, \tag{1.26}$$

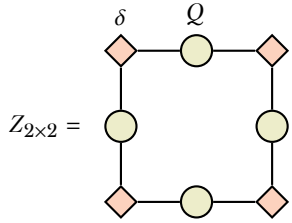

Figure 1.1: A tensor network representation of the partition function of the Ising model on a 2×2 lattice. See Equation 1.23.

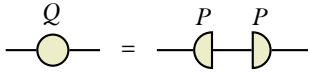

Figure 1.2: Graphical form of Equation 1.25.

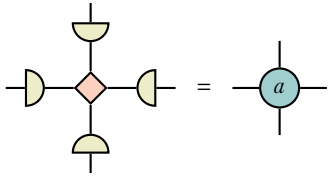

Figure 1.3: Graphical form of Equation 1.26.

where the generalization of the Kronecker delta is defined as

$$\delta_{i_1 \ldots i_n} = \begin{cases} 1 & \text{if } i_1 = \ldots = i_n \\ 0 & \text{otherwise.} \end{cases} \tag{1.27}$$

See Figure 1.3 and Figure 1.4. At the edges and corners, we define suitable tensors of rank 3 and 2, which we will also denote by a:

$$a_{ijk} = \sum_{abc} \delta_{abc} P_{ia} P_{jb} P_{kc},$$
$$a_{ij} = \sum_{ab} \delta_{ab} P_{ia} P_{jb}.$$

The challenge is to approximate this tensor network in the thermodynamic limit.

1.4.3 The transfer matrix as a tensor network

Say something about reshaping legs. It is implicit now.

With our newfound representation of the partition function as a tensor network, we can redefine the row-to-row transfer matrix from Equation 1.16 as the tensor network expressed in Figure 1.5. For all l, it is still true that

$$Z_{N \times l} = \operatorname{Tr} T_N^l = \sum_{i=1}^{2^N} \lambda_i^l, \tag{1.28}$$

so the eigenvalues must be the same. That means that the new definition of the transfer matrix is related to the old one by a basis transformation

$$T_{\text{new}} = P T_{\text{old}} P^T. \tag{1.29}$$

1.5 Transfer matrix renormalization group

There is a deep connection between quantum mechanical lattice systems in d dimensions and classical lattice systems in $d+1$ dimensions. Via the imaginary time path integral formulation, the partition function of a one-dimensional

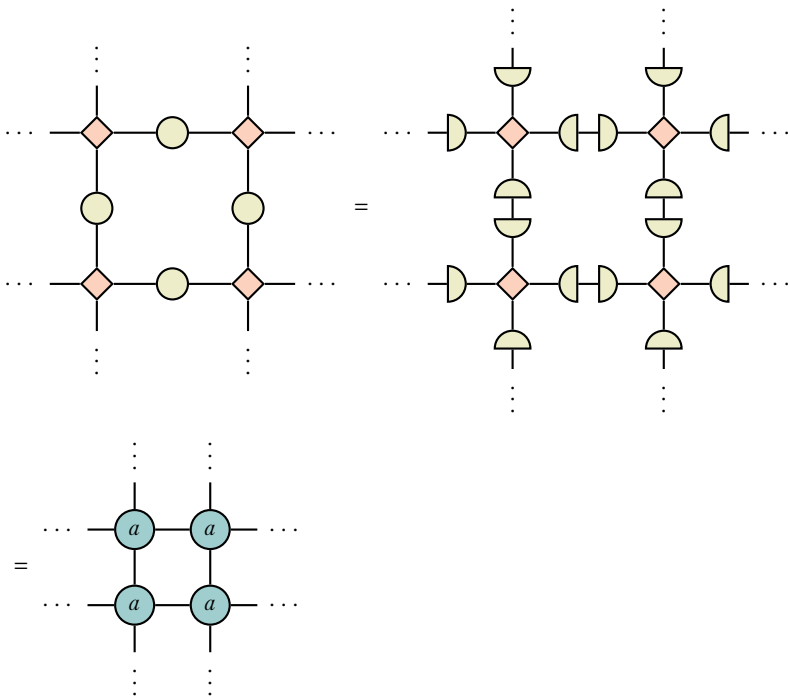

Figure 1.4: $Z_{N\times l}$ can be written as a contracted tensor network of $N \times l$ copies of the tensor a.

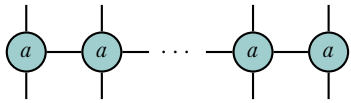

Figure 1.5: The definition of T_N as a network of N copies of the tensor a.

quantum system can be written as the partition function of an effective two-dimensional classical system. The ground state of the quantum system corresponds to the largest eigenvector of the transfer matrix of the classical system.

For more on the quantum-classical correspondence, see ??.

1.5.1 The infinite system algorithm for the transfer matrix

Nishino [1, 2] was the first to apply density matrix renormalization group methods in the context of two-dimensional classical lattices.

Analogous to the infinite system DMRG algorithm for approximating the Hamiltonian of quantum spin chains, our goal is to approximate the transfer matrix in the thermodynamic limit as well as possible within a restriced number of basis states m. We will do this by adding a single site at a time, and truncating the dimension from $2m$ to m at each iteration.

For simplicity, we assume that, at the start of the algorithm, the transfer matrix already has dimension m. We call this transfer matrix P_N. A good choice of initial transfer matrix is obtained by contracting a couple of a-tensors, until dimension m is reached. See Figure 1.6.

To specify fixed instead of open boundary conditions, we may use as boundary tensor a slightly modified version of the three-legged version of a, namely

$$a^{\sigma}_{ijk} = \sum_{abc} \delta_{\sigma abc} P_{ia} P_{jb} P_{kc}, \tag{1.30}$$

that represents an edge site with spin fixed at σ.

We enlarge the system with one site by contracting with an additional a-tensor, obtaining P_{N+1}. See the first network in Figure 1.7.

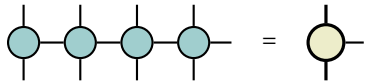

Figure 1.6: A good starting point for the half-row transfer P_N is obtained by contracting a couple of a-tensors, until P_N reaches dimension m.

In order to find the best projection from $2m$ basis states back to m, we embed the system in an environment that is the mirror image of the system we presently have. We call this matrix T_{2N+2}. It represents the transfer matrix of $2N+2$ sites. We find the largest eigenvalue and corresponding eigenvector, as shown in Figure 1.8.

The equivalent of the *reduced density matrix of a block* in the classical case is:

$$\rho_{N+1} = \sum_{\sigma_B} \langle \sigma_B | \lambda_0 \rangle \langle \lambda_0 | \sigma_B \rangle , \tag{1.31}$$

where we have summed over all the degrees of freedom of one of the half-row transfer matrices P_{N+1}. See the first step of Figure 1.9.

The optimal renormalization

$$\widetilde{P}_{N+1} = O P_{N+1} O^\dagger \tag{1.32}$$

is obtained by diagonalizing ρ_{N+1} and keeping the eigenvectors corresponding to the m largest eigenvalues. See the second step of Figure 1.9.

With this blocking procedure, we can successively find

$$P_{N+1} \to P_{N+2} \to \ldots , \tag{1.33}$$

until we have reached some termination condition.

Say something about termination condition.

1.5.2 Physical interpretation of the reduced density matrix

Generalizing the remarks from section 1.3.1 to the two-dimensional case, we see that the normalized lowest-lying eigenvector of the transfer matrix T_N contains the Boltzmann weights of spin configurations on the boundary of a half-infinite $N \times \infty$ lattice.

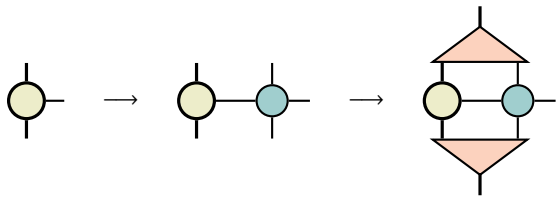

Figure 1.7: In the first step, P_{N+1} is obtained by contracting the current half-row transfer matrix P_N with an additional a-tensor. In the second step, P_{N+1} is truncated back to an m-dimensional matrix, with the optimal low-rank approximation given by keeping the basis states corresponding to the m largest eigenvalues of the density matrix. See Figure 1.9.

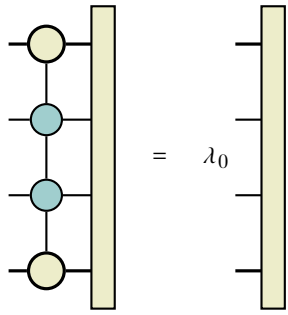

Figure 1.8: Equation for the lowest-lying eigenvector of the row-to-row transfer matrix T_{2N+2}.

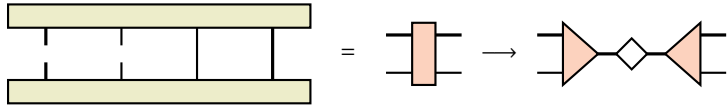

Figure 1.9: Graphical form of Equation 1.31. In the second step, ρ_{N+1} is diagonalized and only the eigenvectors corresponding to the m largest eigenvalues are kept.

Therefore, the classical equivalent of the quantum mechanical reduced density matrix, given by Equation 1.31, and by the first network in Figure 1.9, represents the Boltzmann weights of configurations along a cut in an $N \times \infty$ lattice.

Nishino and Okunishi [2], drawing on ideas from Baxter, realized the Boltzmann weights of configurations along this cut could be obtained by employing *corner transfer matrices*, making it unneccessary to solve the eigenvalue problem in Figure 1.8. Their method, called the Corner Transfer Matrix Renormalization Group method, consumes far less resources while maintaining precision. For this reason, it is the method of choice for most of the simulations in this thesis.

1.6 Corner transfer matrix renormalization group

1.6.1 Corner transfer matrices

The concept of corner transfer matrices for 2D lattices was first introduced by Baxter [**baxter1982exactly**, 3, 4]. Whereas the row-to-row transfer matrix Equation 1.16 corresponds to adding a row to the lattice, the corner transfer matrix adds a quadrant of spins. It was originally defined by Baxter as

$$A_{\boldsymbol{\sigma},\boldsymbol{\sigma}'} = \begin{cases} \sum \prod_{\langle i,j,k,l \rangle} W(\sigma_i, \sigma_j, \sigma_k, \sigma_l) & \text{if } \sigma_1 = \sigma_1' \\ 0 & \text{if } \sigma_1 \neq \sigma_1'. \end{cases} \tag{1.34}$$

Here, the product runs over groups of four spins that share the same face, and the sum is over all spins in the interior of the quadrant.

In a symmetric and isotropic model such as the Ising model, we have

$$W(a, b, c, d) = W(b, a, d, c) = W(c, a, d, b) = W(d, c, b, a) \tag{1.35}$$

and the partition of an $N \times N$ lattice is expressed as

$$Z_{N \times N} = \operatorname{Tr} A^4. \tag{1.36}$$

In the thermodynamic limit, this partition function is equal to the partition function of an $N \times \infty$ lattice, given by Equation 1.17.

The matrix in Equation 1.31, containing the Boltzmann weights of spins along a cut down the middle of an $N \times \infty$ system, is *approximated* by

$$\rho = A^4. \tag{1.37}$$

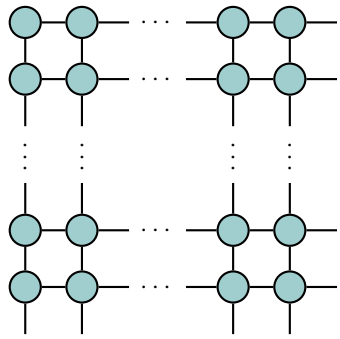

Figure 1.10: Corner transfer matrix expressed as a contraction of a-tensors.

The difference is that A^4 represents a square system of size $N \times N$ with a cut, instead of an $N \times \infty$ strip with a cut. In the thermodynamic limit, both systems become the same. In the corner transfer matrix renormalization group method, A^4 is used to find the optimal projector onto m basis states.

1.6.2 Corner transfer matrix as a tensor network

Similarly to how we redefined the row-to-row transfer matrix (Equation 1.16) as the tensor network in Figure 1.5, we can redefine the corner transfer matrix (Equation 1.34) as the tensor network in Figure 1.10. Again, the new and old definitions of A are related by a basis tranformation

$$A_{\text{new}} = P A_{\text{old}} P^T. \tag{1.38}$$

Something about A being symmetric. What about non-symmetric cases?

1.6.3 Corner transfer matrix renormalization group method

Say something about boundary conditions, also with TMRG algorithm.

The algorithm proceeds very much like the transfer matrix renormalization group method. In addition to renormalizing the half-row transfer matrix P, we also renormalize the corner transfer matrix A at each step, using the projector obtained from diagonalizing A^4.

Compare complexities of both algorithms.

We first initialize P_N and A_N, imposing boundary conditions as we see fit.

We then obtain the unrenormalized A_{N+1} by adding a layer of spins to the quadrant represented by A_N. This is done by contracting with two half-row transfer matrices P_N and a single a-tensor, as shown in the first step of Figure 1.11. We obtain the unnormalized P_{N+1} as before, as shown in the first step of Figure 1.7.

To find the optimal projector from $2m$ to m basis states, we can directly diagonalize A^4_{N+1}, or, equivalently, A_{N+1}. As always, we keep the basis states corresponding to the m largest eigenvectors. This is shown in Figure 1.12. We use the projector to obtain the renormalized versions of A_{N+1} and T_{N+1}

$$\widetilde{A}_{N+1} = O A_{N+1} O^\dagger, \tag{1.39}$$

$$\widetilde{T}_{N+1} = O T_{N+1} O^\dagger. \tag{1.40}$$

shown in the second steps of Figure 1.11 and Figure 1.7.

We repeat the above procedure to successively obtain

$$A_{N+1} \to A_{N+2} \to \ldots, \tag{1.41}$$

$$T_{N+1} \to T_{N+2} \to \ldots \tag{1.42}$$

until a convergence criterion is reached.

Talk about convergence criterion.

1.7 Calculation of observable quantities

To do

1.8 Validity of approximation

To do. Talk about spectrum of reduced density matrix/ctm and how it relates to energy gap/correlation length and critical behaviour.

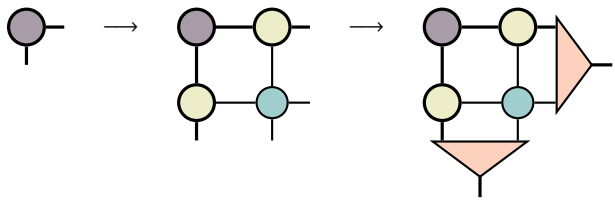

Figure 1.11: In the first step, the unrenormalized A_{N+1} is obtained by contracting with two copies of P_N and a single a-tensor. This corresponds to adding a layer of spins to the quadrant, thus enlarging it from $N \times N$ to $N+1 \times N+1$. In the second step, A_{N+1} is renormalized with the projector obtained from diagonalizing A^4_{N+1} and keeping the basis states corresponding to the m largest eigenvalues.

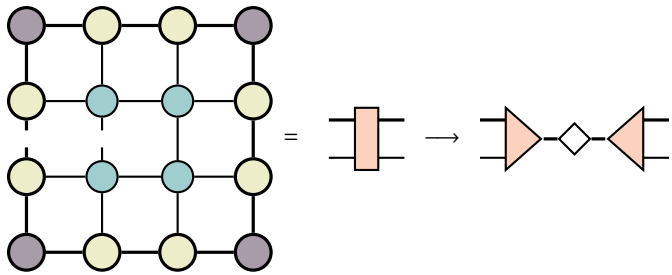

Figure 1.12: The matrix A^4_{N+1} is approximately equal to ρ_{N+1} in Equation 1.31. Compare the graphical forms of this network and the one shown in Figure 1.9. We obtain the optimal projector by diagonalizing A^4_{N+1}, or equivalently A_{N+1}.

1.9 Equivalence to variational approximation in the space of matrix product states.

Talk about Baxter, Rommer and Ostlund, and more recent MPS algorithms. Maybe in appendix?

2

Critical behaviour and finite-size scaling

2.1 Abstract

In this chapter, we introduce the central concepts in critical phenomena and finite-size scaling.

We follow the excellent review by Barber [7] and chapter five of Cardy's book [8].

2.2 Introduction

2.3 Phase transitions

When matter exhibits a sudden change in behaviour, characterized by a change in one or more thermodynamic quantities, we say it undergoes a *phase transition*. A quantity that signifies this change is called an *order parameter*, that can take vastly different forms across systems and transitions. For example, for the transition of a ferromagnet, the order parameter is the net magnetization of the system, while for a percolation transition, it is the size of the largest connected graph.

For a historical account of the classification of phase transitions, see [9]. At the present time, we distinguish between two different types [10].

When some thermodynamic quantity changes discontinuously, i.e. shows a jump, we call the transition *first order*. In contrast, during a *continuous* phase transition a variable undergoes change continuously. The point at which a continuous phase transition occurs, is called the critical point.

The two-dimensional Ising model (*ref here*) in a magnetic field shows both types of transition. At zero magnetic field and $T = T_c = 1/(\log(1 + \sqrt{2}))$, the

magnetization changes from zero for $T > T_c$ to a finite value for $T < T_c$ in a continuous manner.

Below the critical temperature T_c, when the magnetic field h tends to zero from $h > 0$, the magnetization tends to a positive value. Conversely, when the magnetic field tends to zero from $h < 0$, the magnetization tends to a negative value. Thus, across the region $h = 0, T < T_c$ the system undergoes a first-order phase transition.

2.3.1 Finite systems

We will now argue that a phase transition cannot occur in a finite system, but only happens when the number of particles tends to infinity.

Because thermodynamic quantities are averages over all possible microstates of a system, those quantities are completely defined in terms of the system's partition function, or equivalently its free energy.

Since in a finite system, the partition function is a finite sum of exponentials, it is analytic (infinitely differentiable). Hence, thermodynamic quantities cannot show true discontinuities and the phase transitions described in the above section do not occur.

pictures?

2.4 Critical behaviour

We will now focus our attention on continuous phase transitions, more specifically the one that occurs in the two-dimensional Ising model. Before we discuss the behaviour of the free energy around the critical point, we briefly summarize how the thermodynamic limit is approached far away from it. Here, we largely follow [7].

We assume that the free energy per site in the thermodynamic limit

$$f_\infty(T) = \lim_{N\to\infty} \frac{F(T,N)}{N} \tag{2.1}$$

exists, and is not dependent on boundary conditions. By definition, it is not analytic in a region around the critical point.

Outside that region, however, we can write

$$F(T,N) = N f_\infty(T) + o(N), \tag{2.2}$$

where correction terms $g(N)$ of $o(N)$ (little-o of N) obey

$$\lim_{N\to\infty} \frac{g(N)}{N} = 0. \tag{2.3}$$

These corrections, of course, do depend on boundary conditions.

Equation 2.2 is valid only outside the critical region precisely because $F(T, N)$ is analytic *everywhere*, and $f_\infty(T)$ is only analytic away from the critical point.

The behaviour of $F(T, N)$ (and hence, all thermodynamic quantities) at criticality is approached is described by *finite-size scaling*.

2.4.1 Finite-size scaling

Figure 2.1 shows the behaviour of the order parameter obtained by exact diagonalization of the partition function of small lattices. It is clear that far from the critical point, the order parameter is essentially not dependent on system size, while in critical region there are significant deviations from the thermodynamic behaviour.

One can now define two characteristic temperatures [11, 7]. The first being the cross-over temperature T_X at which finite-size effects become important, which is predicted to scale as

$$|T_X - T_c| \propto N^{-\theta}. \tag{2.4}$$

θ is called the cross-over or rounding exponent.

The second characteristic temperature is the pseudocritical temperature, denoted by $T^\star$. It can be defined in several ways, one being the point where the order parameter becomes almost zero (in which case it is the same as the cross-over temperature), or the point where the heat capacity

$$C = T^2 \frac{\partial^2 F}{\partial T^2} \tag{2.5}$$

reaches its maximum. $T^\star$ can be regarded as the point where the finite system in some sense comes closest to undergoing a transition. Generally $T^\star$ will not equal T_X, if only because $T^\star$ depends on boundary conditions: periodic or fixed boundary conditions will nudge the system into an ordered state, therefore $T^\star > T_c$. Free boundary conditions will cause the system to favor disorder and the pseudocritical temperature to be lowered.

In any case, it is predicted that

$$|T^\star - T_c| \propto N^{-\lambda}. \tag{2.6}$$

It is generally accepted that [7]

$$\lambda = \theta. \tag{2.7}$$

Furthermore, if one assumes that finite-size effects become important once the correlation length of the system becomes of order of the system size, i.e. [11]

$$\xi(T_X(N)) \propto N, \tag{2.8}$$

then the correlation length exponent ν, given by

$$\xi(T) \propto |T - T_c|^{-\nu} \tag{2.9}$$

can be related to θ as

$$\theta = \frac{1}{\nu}. \tag{2.10}$$

2.5 Effective length scale related to the bond dimension m

To cite

- [12] original physical derivation of finite-size scaling
- [11] rounding and displacement exponents
- [10] Basic (philosophical) introduction to phase transitions
- [9] Historical account of classification of phase transitions

Todo

- finite-size scaling ansatz, basic scaling laws, data collapse, etc.
- renormalization group derivation? (in appendix?)

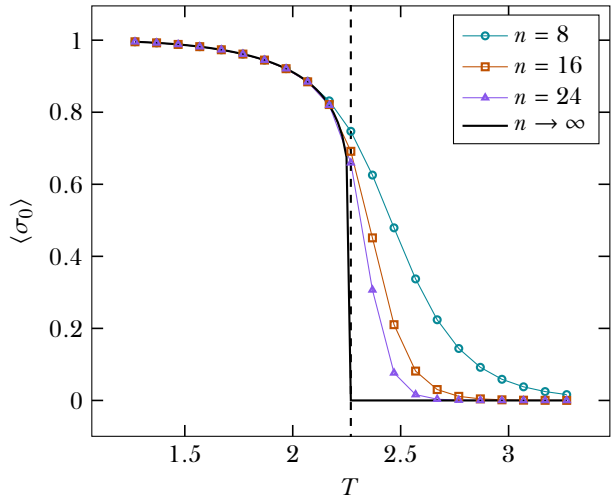

Figure 2.1: The magnetization of the central spin for small lattices with boundary spins fixed to +1. The black line is the exact solution in the thermodynamic limit.

3
Methods

3.1 Abstract

We describe the technical details of the algorithms used to compute quantities of interest. We report the convergence behaviour of the algorithms and discuss validity and sources of error.

3.2 Technical details

For the models treated in this thesis, the corner transfer matrix A and the row-to-row transfer matrix T are symmetric. But due to the accumulation of machine-precision sized errors in the matrix multiplication and singular value decomposition, this will, after many algorithm steps, no longer be the case. In order for results to remain valid, we manually enforce symmetricity after each step.

The tensor network contractions at each algorithm step will cause the elements of A and T to tend to infinity, which means that they will at some point exceed the maximum value of a floating point number as it can be stored in memory. But because the elements of A and T represent Boltzmann weights, they can be scaled by a constant factor, which allows us to prevent this overflow if we use a suitable scaling. For example by requiring that

$$\mathrm{Tr}\, A^4 = 1, \tag{3.1}$$

so that the interpretation of A^4 as a reduced density matrix of an effective one-dimensional quantum is valid.

3.3 Convergence criteria

3.3.1 Simulations with finite bond dimension

The convergence of the CTMRG algorithm with fixed bond dimension m (the infinite system algorithm) can be defined in multiple ways (*cite*). In this thesis, the convergence after step i of the algorithm is defined as

$$c_i = \sum_{\alpha=1}^{m} |s_\alpha^{(i)} - s_\alpha^{(i-1)}|, \tag{3.2}$$

where s_α are the singular values of the corner transfer matrix A. If the convergence falls below some threshold ϵ, the algorithm terminates.

The assumption is that once the singular values stop changing to some precision, the optimal projection is sufficiently close to its fixed point and the transfer matrices A and T represent an environment only limited by the length scale given by m, i.e.

$$\xi(m) \ll N \tag{3.3}$$

is satisfied.

Convergence at the critical point of the Ising model

The convergence is shown in Figure 3.1. It is clear that the phenomenological law

$$\log c_n \propto n \tag{3.4}$$

holds to high precision, with the slope depending on m. Deviations only occur at values of c of around 10^{-12}.

The convergence of the various quantities as function of the number of algorithm steps is shown in Figure 3.2. For all quantities Q, the absolute relative difference with the final algorithm step

$$\Delta Q_{\mathrm{rel}}(n) = \left| \frac{Q(n) - Q(n = 10^5)}{Q(n = 10^5)} \right| \tag{3.5}$$

is shown. Again, a law of the form

$$\log(\Delta Q_{\mathrm{rel}}) \propto n \tag{3.6}$$

seems to hold.

To make an estimate of a quantity in the limit $N \to \infty$, or equivalently $\epsilon \to 0$, we can study the change in a quantity as function of the convergence threshold ϵ. We define

$$\Delta Q(\epsilon) = Q(\epsilon) - Q(10\epsilon), \tag{3.7}$$

i.e. the change of quantity Q when we decrease the threshold ϵ by an order of magnitude. The results in Figure 3.3 show that, remarkably, the order parameter, entropy and correlation length to high precision follow the linear relationship

$$\Delta Q(\epsilon) = \alpha_1(m)\epsilon, \tag{3.8}$$

whereas the free energy follows a quadratic relationship

$$\Delta f(\epsilon) = \alpha_2(m)\epsilon^2. \tag{3.9}$$

This means that we can confidently extrapolate the value of a quantity in the fully converged limit as

$$Q(\epsilon \to 0) = Q(\epsilon_{\min}) + \sum_{\epsilon = \frac{\epsilon_{\min}}{10}, \frac{\epsilon_{\min}}{100}, \ldots} \Delta Q(\epsilon), \tag{3.10}$$

where $\epsilon_{\min}$ is the lowest threshold used in simulation, and $\Delta Q(\epsilon)$ is determined by fitting to suitable higher values of the threshold.

technically this is not correct for the already converged values of m

Cross check with correlation length, report on boundary conditions

3.3.2 Simulations with finite system size

In the finite-system algorithm, we want to reliably extrapolate quantities in the bond dimension m. The convergence behaviour is shown in Figure 3.4. For each quantity Q, we plot the absolute relative difference with the value at the highest m

$$\Delta Q_{\text{rel}}(m) = \left| \frac{Q(m) - Q(m = 200)}{Q(m = 200)} \right| \tag{3.11}$$

versus the bond dimension m.

The plateaus of m-values that barely increase the precision are due to the structure in the spectrum of the reduced density matrix. Apart from this noise, the law

$$\Delta Q_{\text{rel}}(m) \propto m^{\alpha(N)} \tag{3.12}$$

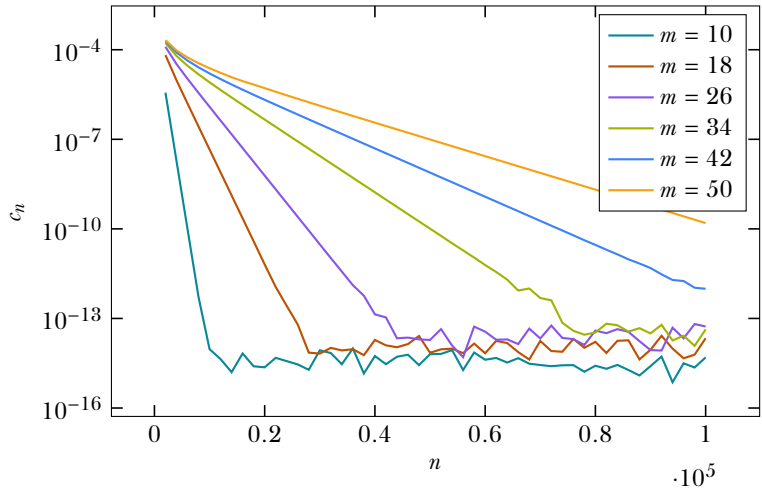

Figure 3.1: Convergence as defined in Equation 3.2 versus n, the number of CTMRG steps. Up until very small values of c_n, the convergence is monotonically decreasing and obeys a logarithmic law with slope depending on m.

is seen to hold for high enough m for the order parameter, free energy and entropy.

Why does the free energy converge much faster?

To extrapolate to $m \to \infty$, analogously to the finite-m case we define

$$\Delta Q_{\text{step}}(m) = Q(m) - Q(m-1), \tag{3.13}$$

which is plotted in the left panel of Figure 3.5. As expected from Equation 3.12, the overall trend looks like a power law, but the noise makes it hard to determine it accurately. It is anyway neither practical nor needed to calculate a system of finite size for many consecutive values of m, in order to get a good approximation to Equation 3.13.

As described in (*ref here to section about spectrum*) and in [13, 14, 15], for the off-critical Ising model the degeneracies in the corner transfer matrix A are exactly known. These degeneracies are smoothed out, but not completely lost

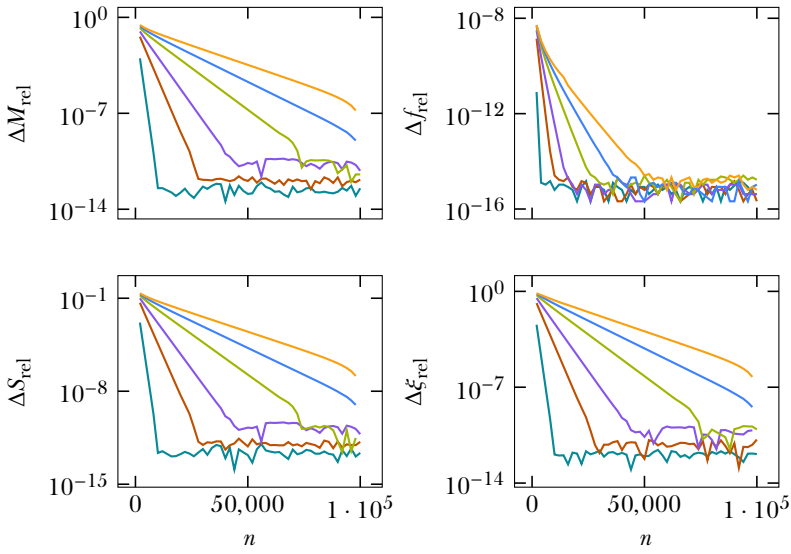

Figure 3.2: Absolute relative difference of quantities (see Equation 3.5). Same legend as Figure 3.1.

for finite systems near criticality. This is directly related to the convergence of quantities in m. The right panel of Figure 3.5 shows the convergence using only the values of m for which all basis states with a certain energy level are present, i.e. [13]

$$m(j) = \sum_{k=0}^{k=j} p(k). \tag{3.14}$$

The first few values of $m(j)$ are

$$1, 2, 3, 5, 7, 10, 14, 19, 25, 33, 43, 55, 70, 88, 110, 137, 169, 207, \ldots \tag{3.15}$$

Using these values of m, the noise largely disappears, but the convergence behaviour is still not devoid of structure entirely.

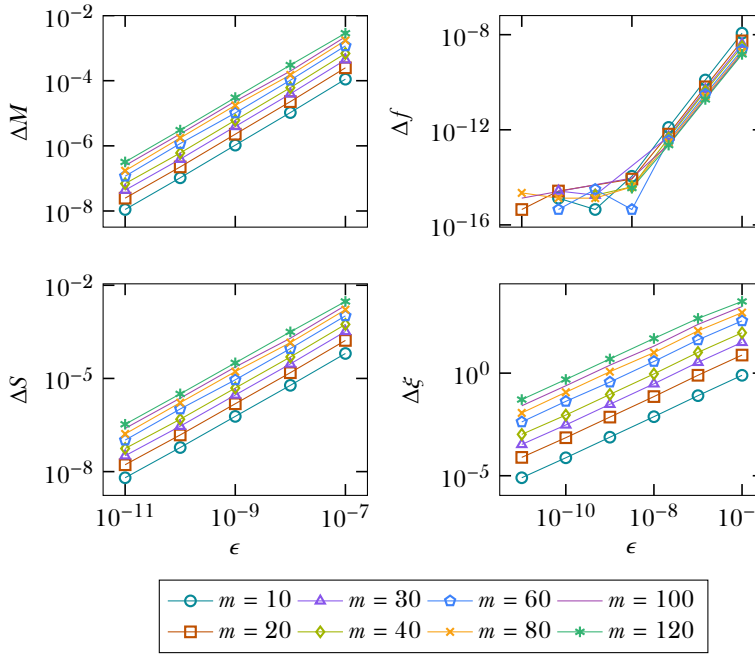

Figure 3.3: Stepwise differences upon decreasing the threshold ϵ by an order of magnitude, as in Equation 3.7. For the order parameter, entropy and correlation length, a linear relationship holds to high precision, while for the free energy the relationship is quadratic.

Nevertheless, the error on a quantity calculated at bond dimension $m_{\max}$ can be approximated as

$$M(m \to \infty) = \sum_{m=m_{\max}+1}^{\infty} \Delta Q_{\text{step}}(m), \tag{3.16}$$

where ΔQ_{step} is fitted from aptly chosen lower values of m.

Make connection with paper by Calabrese and Lefevre?

3.4 Spectrum of the corner transfer matrix

3.4.1 Analytical results for the Ising model

In what follows, we present results established in [15, 16].

For the off-critical Ising model on a square lattice, we have [14]

$$\hat{\rho} = \hat{A}^4 = \exp(-\hat{H}_{\text{CTM}}), \tag{3.17}$$

where

$$\hat{H}_{\text{CTM}} = \sum_{l=0}^{\infty} \epsilon_l(T) c_l^\dagger c_l, \tag{3.18}$$

with c_l and $c_l^\dagger$ fermionic annihilation and creation operators and

$$\epsilon_l = \begin{cases} (2l+1)\epsilon(T) & \text{if } T > T_c, \\ 2l\epsilon(T) & \text{if } T < T_c. \end{cases} \tag{3.19}$$

with $\epsilon(T)$ a model-specific factor that only depends on temperature.

In other words, the reduced density matrix (or equivalently, the corner transfer matrix A) can be written as a density matrix of an effective free fermionic Hamiltonian with equally spaced excitations.

What does this mean for the spectrum of A? If we assume a free boundary, we have to distinguish between the ordered and disordered phase.

In the disordered phase, we have $\epsilon_l = (2l+1)\epsilon(T)$. The ground state, $E = 0$, corresponds to the vacuum state of the effective system described by H_{CTM}. The single-fermion excitations give ϵ, 3ϵ, 5ϵ, ..., while two-fermion excitations give 4ϵ ($c_0^\dagger c_1^\dagger |0\rangle$), 6ϵ ($c_0^\dagger c_2^\dagger |0\rangle$) and 8ϵ ($c_0^\dagger c_3^\dagger |0\rangle$ *or* $c_1^\dagger c_2^\dagger |0\rangle$). So the

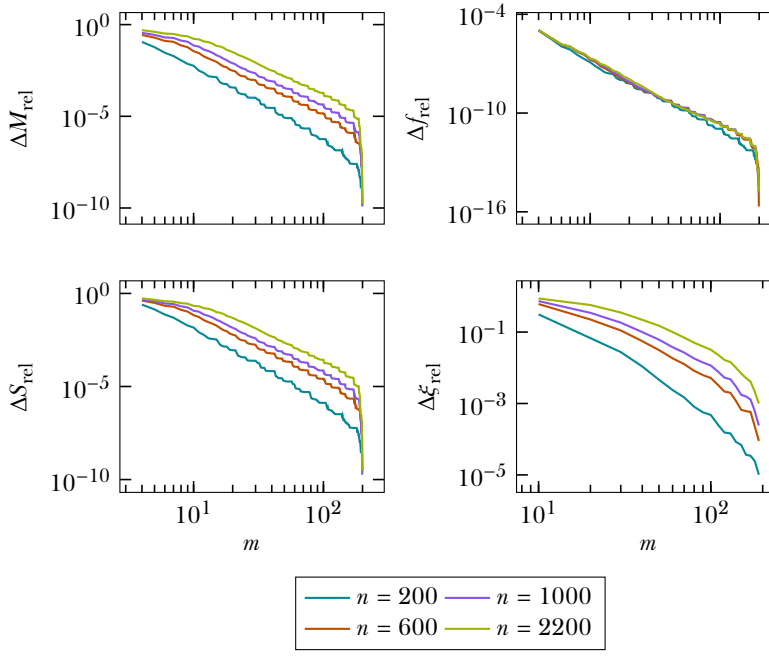

Figure 3.4: The absolute relative difference of quantities, as defined in Equation 3.11. For high enough m, it obeys a power law with varying exponent $\alpha(N)$. The sharp drop for the highest values of m is an artefact of the definition of ΔQ_{rel} and the plateau-like fashion in which the value of a quantity converges, owing to the spectrum of the reduced density matrix approximated by the CTMRG algorithm. Like in the finite-m case, the free energy converges much faster than the other quantities, and does so with little n-dependence. Note that $\Delta\xi_{\mathrm{rel}}$ does not obey a power law.

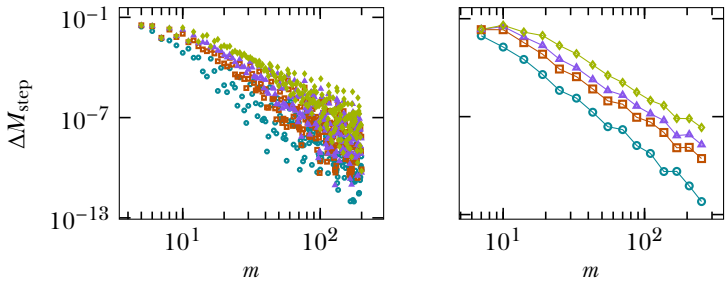

Figure 3.5: Same legend as Figure 3.4

first degeneracy appears at 8ϵ. 9ϵ is also degenerate: it can be constructed with a single-fermion excitation ($c_4^\dagger |0\rangle$) and a three-fermion excitation ($c_2^\dagger c_1^\dagger c_0^\dagger |0\rangle$).

The numerical results from the CTMRG algorithm exactly confirm this picture. See the $T = 2.6$ line in the left panel of Figure 3.6. The gap after the first two eigenvalues is due to the absence of the level 2ϵ. The ϵ_l are linear and the degeneracies are correct.

In the ordered phase, we have a two-fold degeneracy for every state due to symmetry and ground state energy $E = 0$. After that, the only available levels are 2ϵ, 4ϵ, 6ϵ, ... The degeneracy of the nth energy level is given by $2p(n)$, twice the number of partitions of n into distinct integers [13], with the factor of two coming from symmetry.

To illustrate: $c_1^\dagger c_2^\dagger |0\rangle$ and $c_3^\dagger |0\rangle$ both have $E = 6\epsilon$, the third energy level (counting the vacuum as the zeroth energy level), which is to say $p(3) = 2$ since $\{3, 2 + 1\}$ are the ways to write 3. The line $T = 2$ in the left panel of Figure 3.6 confirms these results.

With a fixed boundary, the spectrum in the disordered phase doesn't change. In the ordered phase however, the two-fold degeneracy due to symmetry is lifted, so the degeneracy of the nth energy level becomes $p(n)$. As a consequence, the spectrum decays much faster. See the right panel of Figure 3.6.

At or close to criticality, the expression in Equation 3.17 breaks down, and the spectrum of $\hat{\rho}$ is smoothened out. In general, below and at criticality, the spectrum decays slower for a free boundary. This is to be expected, since A preserves the symmetry when the boundary is free. At $T = 0$, A has two equally large non-zero eigenvalues, representing either all up or all down spins

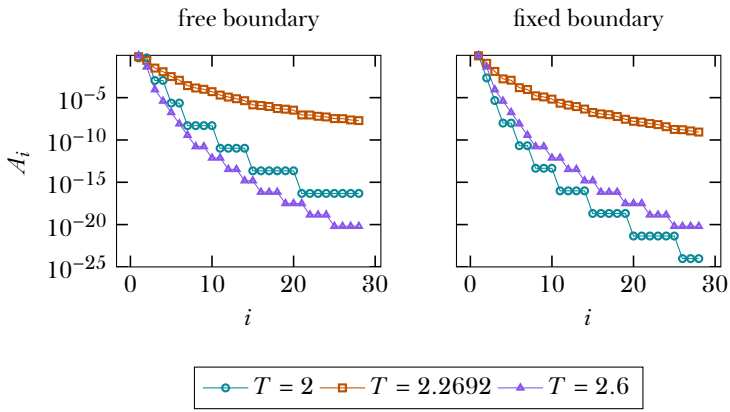

Figure 3.6: First part of the spectrum of A after $n = 1000$ steps with a bond dimension of $m = 250$.

on the boundary of the quadrant, while for a fixed boundary, A has one non-zero eigenvalue: it represents a completely polarized state.

4
Results

4.1 Abstract

Cite more

We present finite-size scaling results using the corner transfer matrix renormalization group method on two-dimensional classical square lattices [2]. We compare the results of conventional finite-size scaling in the system size N with scaling in the number of states kept during the renormalization step of the algorithm, denoted by m. Such a comparison was first done in [17]. We highlight the areas in which method excels over the other.

Calculate critical temperature and exponents using information that is directly extractable from the corner transfer matrix.

4.2 Introduction

The first direct comparison of finite-size scaling in the system size N with scaling in the bond dimension of the corner transfer matrix renormalization group method m was done in [17]. In explaining the basic concepts, we largely follow this paper.

The error in the approximation of the partition function (and thus all thermodynamic quantities) in the thermodynamic limit with the corner transfer matrix method depends on two characteristic length scales. The first is the size of the system N. After n steps of the infinite-system algorithm, we have

$$N = 2n + 1. \tag{4.1}$$

The second length scale is related to the finite bond dimension m. Baxter [4], and later Östlund and Rommer [18] (in the context of one-dimensional quantum systems) showed that in the thermodynamic limit, CTMRG and

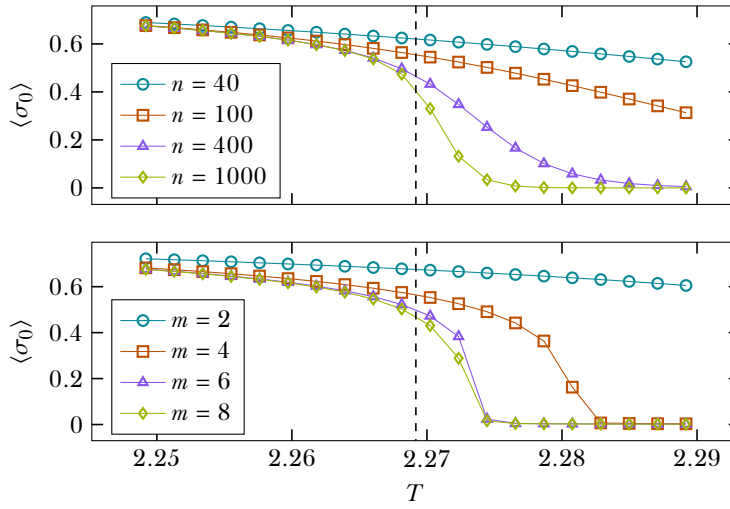

Figure 4.1: Upper panel: expectation value of the central spin $\langle\sigma_0\rangle$ after n CTMRG steps. m is chosen such that the truncation error is smaller than 10^{-6}. Lower panel: $\langle\sigma_0\rangle$ for systems with bond dimension m.

DMRG are variational optimizations in the space of matrix product states.

Can extend this idea a bit.

It is known that an MPS-ansatz with finite bond dimension inherently limits the correlation length of the system to a finite value [19]. Hence, thermodynamic quantities obtained from the CTMRG algorithm with finite m, in the limit $N \to \infty$, cannot diverge and must show finite-size effects similar to those of some effective finite system of size $N_{\text{eff}}(m)$ depending on the bond dimension m.

Figure 4.1 shows the behaviour of the order parameter of the two-dimensional Ising model for systems of finite-size, where m has been chosen such that the truncation error is smaller than 10^{-6}, and for systems of finite m, where the result is converged in the system size N. The results look very similar and support the above claim.

Order parameter is not the same as magnetization central spin. Where to explain this?

4.2.1 Definition of N_{eff} in terms of the correlation length at T_c

In the thermodynamic limit (corresponding to infinite m and N), we have the following expression for the correlation length of a classical system [20]

$$\xi(T) = \frac{1}{\log\left(\frac{T_0}{T_1}\right)}. \tag{4.2}$$

Here, T_0 and T_1 are the largest and second-largest eigenvalues of the row-to-row transfer matrix T, respectively. With N tending towards infinity and finite m, near the critical point $\xi(T)$ should obey a scaling law of the form

$$\xi(T, m) = N_{\text{eff}}(m)\mathcal{F}(N_{\text{eff}}(m)/\xi(T)) \tag{4.3}$$

with

$$\mathcal{F}(x) = \begin{cases} \text{const} & \text{if } x \to 0, \\ x^{-1} & \text{if } x \to \infty. \end{cases} \tag{4.4}$$

Hence, the effective length scale corresponding to the finite bond dimension m is proportional to the correlation length of the system at the critical point $t = 0$.

$$N_{\text{eff}}(m) \propto \xi(T = T_c, m). \tag{4.5}$$

Under this assumption, the order parameter should obey the following scaling relation at the critical temperature

$$M(T = T_c, m) \propto \xi(T = T_c, m)^{-\beta/\nu}. \tag{4.6}$$

The left panel of Figure 4.2 shows that this scaling relation holds. The fit yields $\frac{\beta}{\nu} \approx 0.125(5)$, close to the true value of $\frac{1}{8}$.

The right panel shows the conventional finite-size scaling relation

$$M(T = T_c, N) \propto N^{-\beta/\nu}, \tag{4.7}$$

yielding $\beta/\nu \approx 0.1249(1)$, which can be systematically improved by fitting to larger system sizes, obtained with a fixed truncation error.

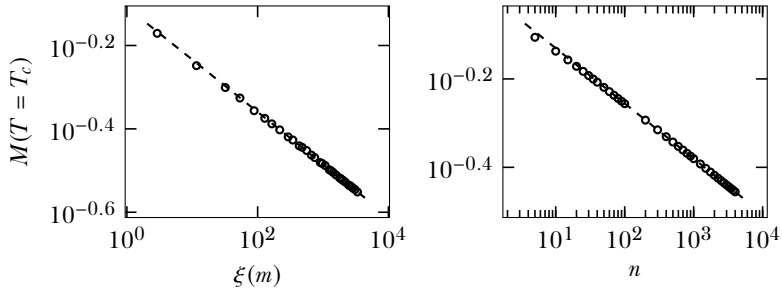

Figure 4.2: Left panel: fit to the relation in Equation 4.6, yielding $\frac{\beta}{\nu} \approx 0.125(5)$. The data points are obtained from simulations with $m = 2, 4, \ldots, 64$. The smallest 10 values of m have not been used for fitting, to diminish correction terms to the basic scaling law. Right panel: fit to conventional finite-size scaling law given in Equation 4.7.

In the case of scaling in correlation length $\xi(m)$, the exponent does not improve when taking bigger values of m, while keeping the termination criterion (relative change of singular values) fixed. This points to a flaw in the termination criterion of the algorithm.

Furthermore, the correlation length $\xi(m)$ shows characteristic half-moon patterns on a log-log scale, stemming from the degeneracies in the corner transfer matrix spectrum. This makes the data harder to interpret, since the effect of increasing m depends on how much of the spectrum is currently retained.

Talk about how to alleviate this partially by using entropy S as length scale.

To further test the hypothesis that N and $\xi(m)$ are the only relevant length scales, the authors of [17] propose a scaling relation for the order parameter M at the critical temperature of the form

$$M(N, m) = N^{-\beta/\nu} \mathcal{G}(\xi(m)/N) \tag{4.8}$$

with

$$\mathcal{G}(x) = \begin{cases} \text{const} & \text{if } x \to \infty, \\ x^{-\beta/\nu} & \text{if } x \to 0, \end{cases} \tag{4.9}$$

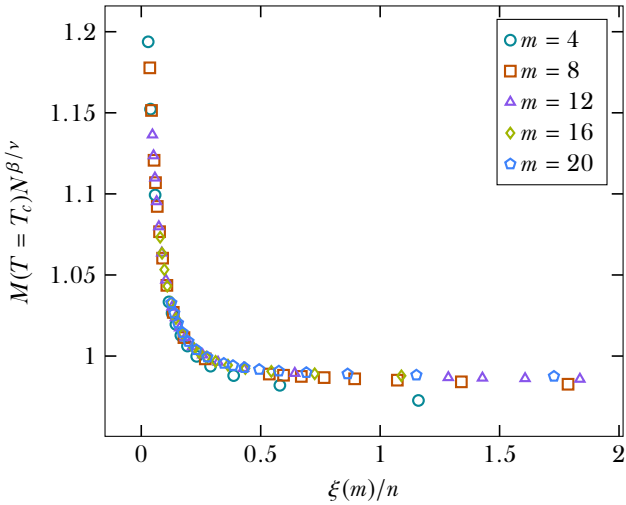

Figure 4.3: Scaling function $\mathcal{G}(\xi(m)/N)$ given in Equation 4.8.

meaning that Equation 4.8 reduces to Equation 4.7 in the limit $\xi(m) \gg N$ and to Equation 4.6 in the limit $N \gg \xi(m)$. Figure 4.3 shows that the scaling relation of Equation 4.8 is justified.

Figure 4.4 shows the cross-over behaviour from the N-limiting regime, where $M(N, m) \propto N^{-\beta/\nu}$ to the $\xi(m)$-limiting regime, where $M(N, m)$ does not depend on N.

4.2.2 Scaling relations away from the critical point

In general, the position of the critical point is not known. In that situation, the scaling relation in Equation 4.8 cannot be used to calculate thermodynamic information. Instead, in the limit $N \to \infty$, we should have

$$M(t, m) \propto \xi(m)^{-\beta/\nu} \mathcal{P}(t\xi(m)^{1/\nu}), \tag{4.10}$$

which is confirmed in Figure 4.5.

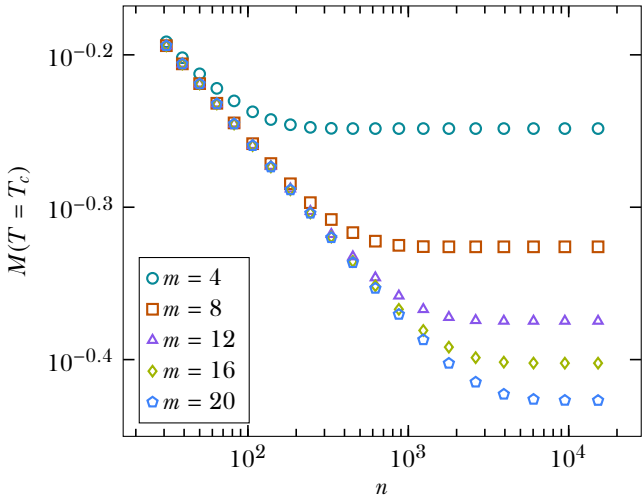

Figure 4.4: Behaviour of the order parameter at fixed m as function of the number of renormalization steps n. For small n, all curves coincide, since the system size is the only limiting length scale. For large enough n, the order parameter is only limited by the length scale $\xi(m)$. In between, there is a cross-over described by $\mathcal{G}(\xi(m)/N)$, given in Equation 4.8.

However, in practice this is still problematic, since $\xi(m)$ is defined at the critical point. Thus, we must find a way to define the length scale corresponding to a finite bond dimension m without making use of the position of the critical point.

4.3 Finite-entanglement scaling and its relation to two-dimensional classical lattices

Another way to understand the fact that the CTMRG method with finite m can never accurately represent systems at criticality, is by looking at the entanglement properties of the ground state of the corresponding one-dimensional quantum systems.

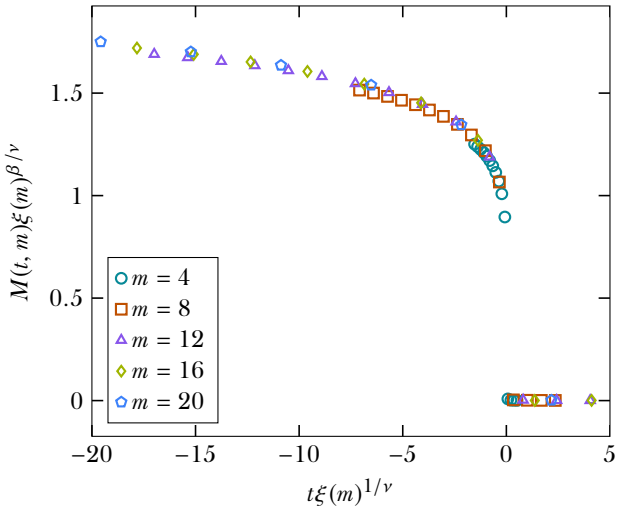

Figure 4.5: Scaling function $\mathcal{P}(t\xi(m)^{1/\nu})$ in Equation 4.10.

It is known that near the critical point, when the correlation length ξ is large but finite, the entanglement of a subsystem A scales as

$$S_A \propto \mathcal{A}(c/6)\log(\xi) \tag{4.11}$$

where $\mathcal{A}$ is the number of boundary points of A and c is the central charge of the conformal field theory at the critical point [21, 22, 23].

Recalling the definition of the entanglement entropy

$$S_A = -\operatorname{Tr}(\rho_A \log \rho_A) = -\sum_\alpha \omega_\alpha \log \omega_\alpha, \tag{4.12}$$

it is trivially seen that the entropy of a state given by the DMRG (or any other MPS), which only retains m basis states of ρ_A, is limited by

$$S_A^{\max}(m) = \log m \tag{4.13}$$

by putting $\omega_\alpha = 1/m$ for $\alpha = 1, \ldots, m$.

Empirically, MPS ground states of critical systems do not reach their maximum entropy $\log m$, but one may still assume

$$S_A \propto S_A^{\max}(m) \tag{4.14}$$

close to criticality, which directly implies the relationship

$$\xi(m) \propto m^{\kappa}. \tag{4.15}$$

Numerical evidence of this fact was first given by the authors of [24], who found

$$\xi(m) \propto m^{1.3} \tag{4.16}$$

for a gapless system of free fermions, using DMRG calculations. Later, using the iTEBD algorithm [25], the authors of [26] presented numerical evidence for such a relation for the Ising model with transverse field and the Heisenberg model, with

$$\kappa_{\text{Ising}} \approx 2, \tag{4.17}$$

$$\kappa_{\text{Heisenberg}} \approx 1.37. \tag{4.18}$$

A quantitative theory of this behaviour was given in [27]. Assuming the energy density as function of the effective correlation length ξ takes the form

$$E(\xi) = E_\infty + \frac{A}{\xi^2} + \frac{B}{\xi} P_r(m), \tag{4.19}$$

where

$$P_r(m) = \sum_{\alpha=m}^{\infty} \omega_\alpha \tag{4.20}$$

is the residual probability. Using results in [28] for the spectrum of ρ_A in limit $m \to \infty$, ξ is found to obey Equation 4.15 with

$$\kappa = \frac{6}{c(\sqrt{12/c} + 1)} + \mathcal{O}(1/\log m), \tag{4.21}$$

yielding

$$\kappa_{\text{Ising}} = 2.034\ldots, \tag{4.22}$$

$$\kappa_{\text{Heisenberg}} = 1.344\ldots, \tag{4.23}$$

which are in good agreement with the findings in [26].

4.3.1 Classical analogue of entanglement entropy

The key point of the corner transfer matrix renormalization group method [29, 2] is that it unifies White's density matrix renormalization group method [5] with Baxter's corner transfer matrix approach [3, 4], through the identification (in the isotropic case)

$$\rho_{\text{half-chain}} = A^4. \tag{4.24}$$

This allows one to define a 2D classical analogue to the half-chain entanglement entropy of a 1D quantum system

$$S_{\text{classical}} = -\operatorname{Tr} A^4 \log A^4 = -\sum_{\alpha=1}^{m} \nu_\alpha^4 \log \nu_\alpha^4, \tag{4.25}$$

where ν_α are the eigenvalues of the corner transfer matrix A. In the CTMRG algorithm, A is kept in diagonal form, making $S_{\text{classical}}$ trivial to compute.

In [30], numerical evidence is given for the validity of Equation 4.25 for a wide range of models, and the concept is generalized to higher dimensions. For an overview of applying corner transfer matrices in higher dimensions and to quantum systems, see [31].

4.3.2 Locating the critical point with the entanglement spectrum

Since phase transitions of quantum systems can be located by studying their entanglement spectrum (*cite here*), classical systems may be investigated in the same way through the correspondence in Equation 4.24. This is an alternative to the usual approach of studying an order parameter or derivatives of thermodynamical observables (*cite here?*).

Examples of studies using the spectrum of the corner transfer matrix to analyze two-dimensional classical systems are [32, 33, 34].

- [30]: refs [42] and [12] contain many papers which study the phenomenon of pinpointing a phase transition without using physical observables (i.e. entanglement, spectrum, fidelity instead.)
- [35]: for XY and Ising model, proves that next-to-nearest neighbor entanglement peaks at critical point (though not nearest-neighbor entanglement.)

4.3.3 Numerical results

We now check the validity of Equation 4.15 in the context of the CTMRG method for two-dimensional classical systems. Similar checks were done for one-dimensional quantum systems in [26].

Directly checking Equation 4.15 yields $\kappa = 1.93$, see top left panel of Figure 4.6. Under the assumption of Equation 4.15, we have the following scaling laws at the critical point

$$M(m) \propto m^{-\beta\kappa/\nu} \tag{4.26}$$

$$f(m) - f_{\text{exact}} \propto m^{(2-\alpha)\kappa/\nu} \tag{4.27}$$

for the order parameter and the singular part of the free energy, respectively. A fit to $M(m)$ yields $\kappa = 1.93$ and a fit to $f(m) - f_{\text{exact}}$ yields $\kappa = 1.90$. See the top right and bottom left panels of Figure 4.6. Here, we have used $\beta = 1/8$, $\nu = 1$ and $\alpha = 0$ for the Ising model.

Tell that the κ law is indeed valid, since it is a good fit.

We may use Equation 4.11 and Equation 4.25 to check the relation

$$S_{\text{classical}} \propto \frac{c\kappa}{6} \log m, \tag{4.28}$$

which also yields $\kappa = 1.93$, where $c = 1/2$ for the Ising model. See bottom right panel of Figure 4.6.

We may directly verify the value of the central charge c associated with the conformal field theory at the critical point by fitting to

$$S_{\text{classical}} \propto \frac{c}{6} \log \xi(m), \tag{4.29}$$

which yields $c = 0.501$, shown in the left panel of Figure 4.7.

The right panel of Figure 4.7 shows the fit to the scaling relation in N (or, equivalently the number of CTMRG steps n)

$$S_{\text{classical}} \propto \frac{c}{6} \log N, \tag{4.30}$$

which yields $c = 0.498$.

To verify if the point of maximum entropy

$$T^\star(m) = \max_T S(T, m) \tag{4.31}$$

is a good definition of the pseudocritical point, we fit the relation

$$T^\star - T_c \propto \xi(m)^{-1/\nu}. \tag{4.32}$$

which yields $\widetilde{T}_c = 2.2692$ and $\nu = 0.997$ when the length scale $\xi(T^\star, m)$ is used, shown in the left panel of Figure 4.8. Here, $\widetilde{T}_c$ denotes the critical temperature found by minimising the norm of squares of a fit of the form given in Equation 4.32. In finding the position of the pseudoccritical temperature $T^\star$, a tolerance of 10^{-6} was used.

If, however, the length scale $\xi(m, T_c)$ at the actual critical point is used, a much worse fit is obtained, yielding $\widetilde{T}_c = 2.2691$ and $\nu = 0.90$, shown in the right panel of Figure 4.8.

This signifies the value of $\xi(T^\star, m)$ is heavily dependent on $T^\star$, and using the length scale at the actual pseudocritical temperature found somehow offsets the error on its position.

this is unclear.

Assuming Equation 4.15, Equation 4.32 becomes

$$T^\star - T_c \propto m^{-\kappa/\nu}, \tag{4.33}$$

which yields *values*, shown in the bottom left panel of Figure 4.8.

As a cross check, we can fit instead to scaling relation of the pseudocritical temperature for finite N

$$T^\star - T_c \propto N^{-1/\nu}, \tag{4.34}$$

yielding *values*. See the bottom right panel of Figure 4.8.

- validate pseudocritical point by matching it to pseudocritical point given by correlation length and magnetization (how?)
- scaling of pseudocritical point $T^\star - T_c \propto m^{-\kappa/\nu}$.

4.4 To do

Articles to cite:

- [36]: assumes existence of κ and compares finite-size scaling with finite-m scaling for 1D quantum systems with periodic boundary conditions.
- [23]: proves relation for classical eight vertex model

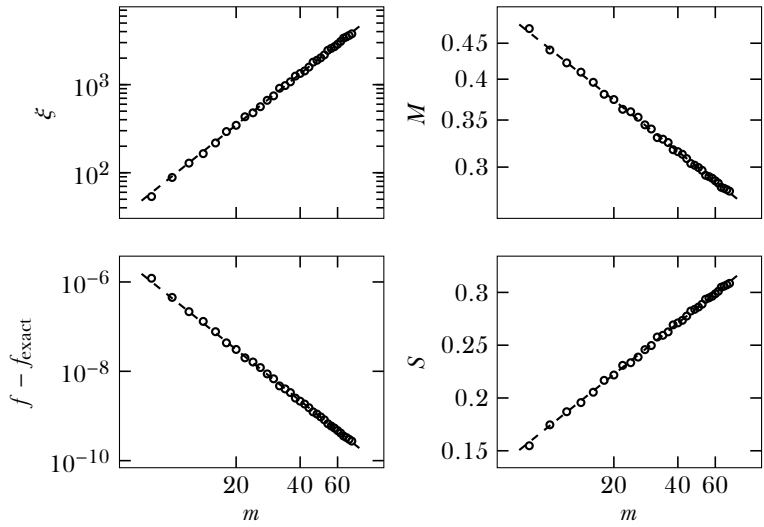

Figure 4.6: Numerical evidence for Equation 4.15, Equation 4.26, Equation 4.28, yielding, from left to right and top to bottom, $\kappa = \{1.93, 1.93, 1.90, 1.93\}$.

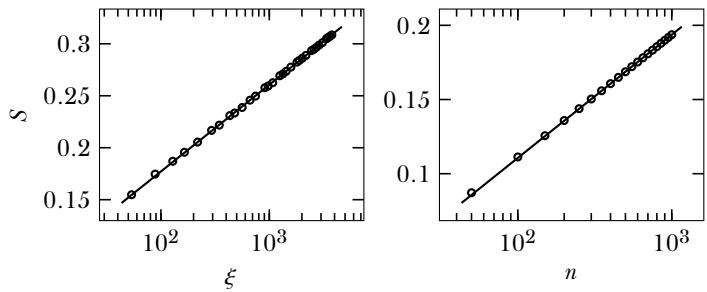

Figure 4.7: Left panel: numerical fit to Equation 4.29, yielding $c = 0.501$. Right panel: numerical fit to Equation 4.30, yielding $c = 0.498$.

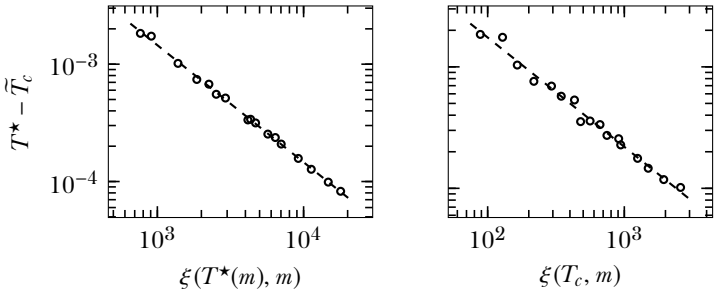

Figure 4.8: Left panel: numerical fit to Equation 4.32 with $\xi(T^\star(m), m)$ used as relevant length scale. Right panel: same fit but using $\xi(T_c, m)$, the correlation length at the exact critical point.

Things to check

- does $S(T^\star, m) \propto \log \xi(T^\star, m)$ hold?
- does $S(T^\star, N) \propto \log N$ hold better than $S(T_c, N) \propto \log N$?
- does fitting $T_c - T^\star(N)$ to N give better results than fitting against $S(T^\star, N)$?
- how does $T^\star(m)$ from entropy compare against $T^\star$ found from max correlation length, or vanishing magnetization?
- optimize κ for scaling of pseudo critical point?
- find $T^{\star,N}$ for larger N for ising model.

Plots to make:

- $T^\star - T_c$ vs N
- $S(T_c, N) \propto \log N$
- generally, why should there be a difference between using entropy at critical point vs using entropy at pseudocritical point? How does each one scale?

Bibliography

[1] Tomotoshi Nishino. "Density matrix renormalization group method for 2D classical models". In: *Journal of the Physical Society of Japan* 64.10 (1995), pp. 3598–3601.

[2] Tomotoshi Nishino and Kouichi Okunishi. "Corner transfer matrix renormalization group method". In: *Journal of the Physical Society of Japan* 65.4 (1996), pp. 891–894.

[3] RJ Baxter. "Dimers on a rectangular lattice". In: *Journal of Mathematical Physics* 9.4 (1968), pp. 650–654.

[4] RJ Baxter. "Variational approximations for square lattice models in statistical mechanics". In: *Journal of Statistical Physics* 19.5 (1978), pp. 461–478.

[5] Steven R White. "Density matrix formulation for quantum renormalization groups". In: *Physical Review Letters* 69.19 (1992), p. 2863.

[6] Ernst Ising. "Beitrag zur theorie des ferromagnetismus". In: *Zeitschrift für Physik* 31.1 (1925), pp. 253–258.

[7] M. N. Barber. "Finite-size Scaling". In: *Phase Transitions and Critical Phenomena*. Ed. by Cyril Domb and J. L. Lebowitz. Vol. 8. Academic press, 1983. Chap. 2.

[8] John Cardy. *Scaling and renormalization in statistical physics*. Cambridge university press, 1996. Chap. 5.

[9] Gregg Jaeger. "The Ehrenfest classification of phase transitions: introduction and evolution". In: *Archive for history of exact sciences* 53.1 (1998), pp. 51–81.

[10] Leo P Kadanoff. "More is the same; phase transitions and mean field theories". In: *Journal of Statistical Physics* 137.5-6 (2009), p. 777.

[11] Michael E Fisher and Arthur E Ferdinand. "Interfacial, boundary, and size effects at critical points". In: *Physical Review Letters* 19.4 (1967), p. 169.

[12] Michael E Fisher and Michael N Barber. "Scaling theory for finite-size effects in the critical region". In: *Physical Review Letters* 28.23 (1972), p. 1516.

[13] Kouichi Okunishi, Yasuhiro Hieida, and Yasuhiro Akutsu. "Universal asymptotic eigenvalue distribution of density matrices and corner transfer matrices in the thermodynamic limit". In: *Physical Review E* 59.6 (1999), R6227.

[14] Brian Davies. "Corner transfer matrices for the Ising model". In: *Physica A: Statistical Mechanics and its Applications* 154.1 (1988), pp. 1–20.

[15] Ingo Peschel and Viktor Eisler. "Reduced density matrices and entanglement entropy in free lattice models". In: *Journal of physics a: mathematical and theoretical* 42.50 (2009), p. 504003.

[16] Ingo Peschel, Matthias Kaulke, and Örs Legeza. "Density-matrix spectra for integrable models". In: *Annalen der Physik* 8.2 (1999), pp. 153–164. ISSN: 1521-3889. DOI: 10.1002/(SICI)1521-3889(199902)8:2<153::AID-ANDP153>3.0.CO;2-N. URL: http://dx.doi.org/10.1002/(SICI)1521-3889(199902)8:2%3C153::AID-ANDP153%3E3.0.CO;2-N.

[17] T Nishino, K Okunishi, and M Kikuchi. "Numerical renormalization group at criticality". In: *Physics Letters A* 213.1-2 (1996), pp. 69–72.

[18] Stellan Östlund and Stefan Rommer. "Thermodynamic limit of density matrix renormalization". In: *Physical review letters* 75.19 (1995), p. 3537.

[19] Michael M Wolf et al. "Quantum phase transitions in matrix product systems". In: *Physical review letters* 97.11 (2006), p. 110403.

[20] Rodney J Baxter. *Exactly solved models in statistical mechanics*. Elsevier, 1982. Chap. 7.

[21] Pasquale Calabrese and John Cardy. "Entanglement entropy and quantum field theory". In: *Journal of Statistical Mechanics: Theory and Experiment* 2004.06 (2004), P06002.

[22] Guifre Vidal et al. "Entanglement in quantum critical phenomena". In: *Physical review letters* 90.22 (2003), p. 227902.

[23] Elisa Ercolessi, Stefano Evangelisti, and Francesco Ravanini. "Exact entanglement entropy of the XYZ model and its sine-Gordon limit". In: *Physics Letters A* 374.21 (2010), pp. 2101–2105.

[24] Martin Andersson, Magnus Boman, and Stellan Östlund. "Density-matrix renormalization group for a gapless system of free fermions". In: *Physical Review B* 59.16 (1999), p. 10493.

[25] Guifre Vidal. "Classical simulation of infinite-size quantum lattice systems in one spatial dimension". In: *Physical review letters* 98.7 (2007), p. 070201.

[26] L Tagliacozzo et al. "Scaling of entanglement support for matrix product states". In: *Physical review b* 78.2 (2008), p. 024410.

[27] Frank Pollmann et al. "Theory of finite-entanglement scaling at one-dimensional quantum critical points". In: *Physical review letters* 102.25 (2009), p. 255701.

[28] Pasquale Calabrese and Alexandre Lefevre. "Entanglement spectrum in one-dimensional systems". In: *Physical Review A* 78.3 (2008), p. 032329.

[29] Tomotoshi Nishino and Kouichi Okunishi. "Corner transfer matrix algorithm for classical renormalization group". In: *Journal of the Physical Society of Japan* 66.10 (1997), pp. 3040–3047.

[30] Ching-Yu Huang, Tzu-Chieh Wei, and Roman Orus. "Holographic encoding of universality in corner spectra". In: *arXiv preprint arXiv:1702.01598* (2017).

[31] Román Orús. "Exploring corner transfer matrices and corner tensors for the classical simulation of quantum lattice systems". In: *Physical Review B* 85.20 (2012), p. 205117.

[32] Roman Krčmár and Ladislav Šamaj. "Reentrant disorder-disorder transitions in generalized multicomponent Widom-Rowlinson models". In: *Physical Review E* 92.5 (2015), p. 052103.

[33] Roman Krcmar, Andrej Gendiar, and Tomotoshi Nishino. "Phase diagram of a truncated tetrahedral model". In: *Phys. Rev. E* 94 (2 Aug. 2016), p. 022134. DOI: 10.1103/PhysRevE.94.022134. URL: https://link.aps.org/doi/10.1103/PhysRevE.94.022134.

[34] Roman Krčmár, Andrej Gendiar, and Tomotoshi Nishino. "Phase transition of the six-state clock model observed from the entanglement entropy". In: *arXiv preprint arXiv:1612.07611* (2016).

[35] Tobias J Osborne and Michael A Nielsen. "Entanglement in a simple quantum phase transition". In: *Physical Review A* 66.3 (2002), p. 032110.

[36] B Pirvu et al. "Matrix product states for critical spin chains: Finite-size versus finite-entanglement scaling". In: *Physical review b* 86.7 (2012), p. 075117.